JOURNAL OF MODERN OPTICS, 2003, VOL. 50, NO. 10, 1563–1572

# Simultaneous frequency conversion and beam shaping for optical-tweezers applications

GABRIEL MOLINA-TERRIZA†, LLUIS TORNER†, STEFANO MINARDI‡ and PAOLO DI TRAPANI‡

† Institute of Photonic Sciences and Department of Signal Theory and Communications, Universitat Politecnica de Catalunya, Gran Capitan UPC-D3, Barcelona, ES 08034, Spain; e-mail: torner@tsc.upc.es

‡ Istituto Nazionale per la Fisica della Materia and Department of Sciences, Università degli Studi dell'Insubria, Via Valleggio 11, I 22100 Como, Italy

(*Received 2 September 2002; revision received 2 October 2002*)

**Abstract.** We review a method which allows the simultaneous frequency-conversion and shaping of a light beam into a variety of patterns. The method is based on the controllable dynamics of vortices nested in the light beams. We outline the theoretical idea behind the technique and discuss experimental observations conducted in SH generation in lithium triborate which demonstrate its feasibility. The technique might find applications in specialized optical tweezers aimed at the wavelength-optimized assembly, fabrication and manipulation of complex microstructures and nanostructures.

## 1. Introduction

With the advent and maturing of optical tweezers technologies [1, 2], areas where shaping of the light tweezers beam might be beneficial are starting to appear, for example, in their applications to nanotechnologies. Important examples include microfabrication and nanofabrication by photopolymerization [3–5], the development of micromachines [6–8], and the assembly and manipulation of complex particle structures [9–13]. In specialized applications, such technologies might also benefit from frequency conversion of the laser light. Recently, we put forward a technique that allows the simultaneous frequency conversion and the shaping of a beam into a variety of light patterns [14–16]. In the case of SH generation (SHG) that is addressed here, the method involves seeded geometries, where both the fundamental frequency pump and weak coherent second-harmonic (SH) seed signals are launched into the frequency-doubling crystal. The new technique is based on the controllable generation of dynamically evolving patterns of frequency-doubled optical vortices [17–22]. Optical vortices are spiral phase ramps around a screw singularity where the phase of the wave is undefined and its amplitude vanishes [23–25]. The order of the dislocation multiplied by its sign is referred to as the winding number, or topological charge, of the dislocation. Vortices can be readily created and nested in light beams, for example, with computer-generated holograms [26, 27].

*Journal of Modern Optics* ISSN 0950–0340 print/ISSN 1362–3044 online 
http://www.tandf.co.uk/journals
DOI: 10.1080/0950340210000579 69

In SHG schemes with moderate powers and wide beams, light undergoes frequency doubling together with the generation of a phase dislocation nested in the SH beam [28, 29]. The topological charge of the dislocation generated is dictated by the charge of the input light. However, a much richer scenario appears in seeded geometries, where the number of vortices existing in the SH beam depends on the features of the pump and seed beams [30], opening the door to the new possibilities discussed here. In section 2 we describe the principle behind the technique and show examples of possible interesting beam-shaping configurations. In section 3 we describe in detail the outcome of experimental demonstration of the technique and present some of the achieved results. In section 4 we summarize our main conclusions.

## 2. Beam shaping in second-harmonic generation

The central idea behind the scheme is to control the number, the location and the dynamic trajectories of all the vortices existing in the SH beam, and hence the zeroes of the amplitude, to modulate the transverse shape of the light intensity. Therefore, the beam modulation in the SHG scheme is to be accomplished through the nucleation and annihilation of vortex–antivortex pairs, and by the dynamic evolution of vortices across the transverse plane of the beam. Snapshots of the evolving beam acquired at different crystal locations thus realize the desired different light intensity distributions. The scheme holds under conditions of low depletion of the pump signal; therefore it can also be realized by the superposition of the generated and corresponding seed SH beams at the end of the crystal instead of at the input. Here we discuss the implementation of the scheme in the seeded SHG geometry, as it appears to be more robust and compact.

When only the fundamental frequency (FF) pump is injected into the crystal under conditions of low depletion and non-critical phase matching, the output SH is a radially symmetric doughnut beam, and thus with no azimuthal intensity variations. The SH beam contains a vortex of topological charge $m_{\mathrm{SH}} = 2\,m_{\mathrm{FF}}$, where $m_{\mathrm{FF}}$ is the topological charge of the vortex nested in the pump beam. However, a completely different scenario appears when the SHG process is seeded with a charged SH input beam. On theoretical grounds the SH output beam can be approximately but accurately constructed in closed form as the superposition of the input seed and the generated SH signals [14, 15, 30]. In the output beam, vortices appear on the locations where the amplitudes of the generated and input beams match. Also, the number of vortices appearing on this radial position is dictated by the relative phases of the individual beams, and so the output SH beam exhibits an $n$-fold azimuthal symmetry, with $n = |2m_{\mathrm{FF}} - m_{\mathrm{SH}}|$. We refer the reader to [10, 11] for the mathematical details.

For a given $n$-symmetry folding, the exact pattern of output light can be varied by controlling the crystal length and the input conditions, such as the intensity and the width of the pump and seed beams. Figure 1 sketches the vortex inventory that is theoretically obtained at the output face of the crystal by solving the evolution equations of seeded SHG under the conditions of our experiments when $m_{\mathrm{FF}} = 0$ and $m_{\mathrm{SH}} = -3$ (see [14, 15] for the full details of the numerical simulations). The diagrammatic sketch shows the location of the existing vortices. They are only to aid the eye; the exact location of the vortices on the beam depends on the particular values of all the parameters involved. When the seed intensity is very weak, there

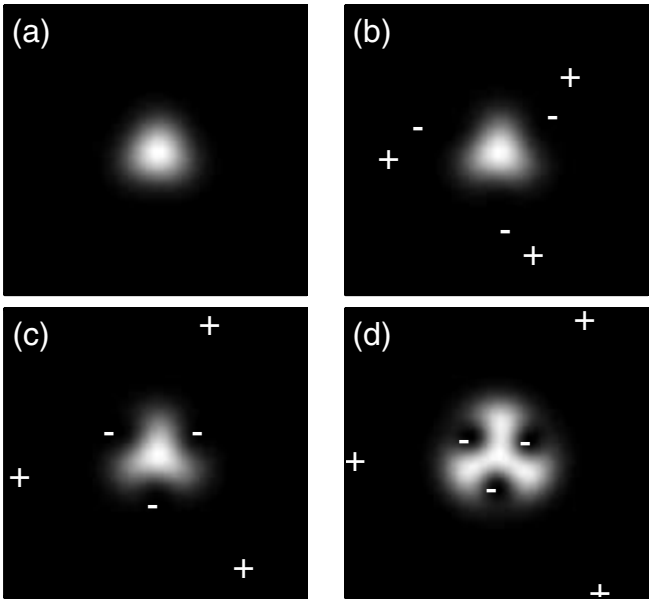


Figure 1. Sketch of the theoretically predicted evolution of all vortices existing under conditions in (*b*), for increasing intensity of the seed signal. Seed intensity increases from (*a*) to (*d*). Plus and minus labels indicate the location of the vortices existing in the light beam. When the seed intensity is very weak, there are no vortices, as in (*a*).

are no vortices in the region shown of the SH beam (figure 1 (*a*)). As the seed intensity increases, vortex twins appear (figure 2 (*b*)). As the intensity is raised further, the vortices with positive charge are located further from the beam axis (figures 1 (*c*) and (*d*)). The vortices with negative charge remain located around the beam waist, and are thus responsible for the dark spots in the intensity distribution.

In figures 2 and 3 we present additional numerical examples, where the beam-shaping effect can be clearly recognized. In these typical examples, by changing the relative amplitude of the beams, it is possible to transform continuously a star-shaped beam into a polygonal structure and vice versa. Therefore, the spatial intensity pattern of the beam can be greatly modified with simple manipulations of the input beams.

The practical potential of the technique relies on the possibility to engineer such superposition directly, by varying the crystal length, the beam widths and the light intensity that is launched into the crystal. Thus, provided that one can control the relative amplitudes of the beams, one can obtain a complex intensity pattern, which can be dynamically controlled in order, for example, to manipulate a pattern of particles or colloids, or to arrange series of micromachines in a certain manner. Such reconfigurable patterns can also be used as the pump light beam for the fabrication by photopolymerization.

## 3. Experimental results

Our set-up (figure 4) was arranged to launch collinearly and coaxially both a FF beam and a SH beam into a lithium triborate (LBO) $LiB_3O_5$ crystal 30 mm

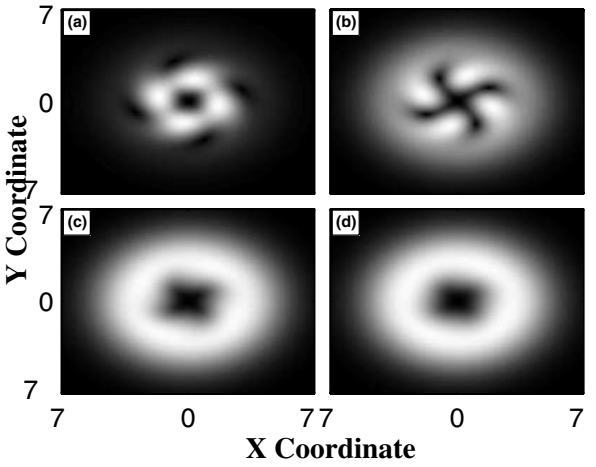


Figure 2. Representative examples of the patterns of SH light that are numerically obtained by changing the amplitude of the input SH seed, where the simulations correspond to the triangles of figure 1 (conditions: crystal length is one FF Rayleigh length; amplitude of the pump beam, $A_{\mathrm{FF}} = 0.1$; width of the pump beam, $w_{\mathrm{FF}} = 2$; SH input beam width, $w_{\mathrm{FF}} = 3$; input topological charges, $[m_{\mathrm{FF}}, m_{\mathrm{SH}}] = [1, -2]$): (*a*) $A_{\mathrm{SH}} = 0.005$; (*b*) $A_{\mathrm{SH}} = 0.01$; (*c*) $A_{\mathrm{SH}} = 0.05$; (*d*) $A_{\mathrm{SH}} = 0.1$.

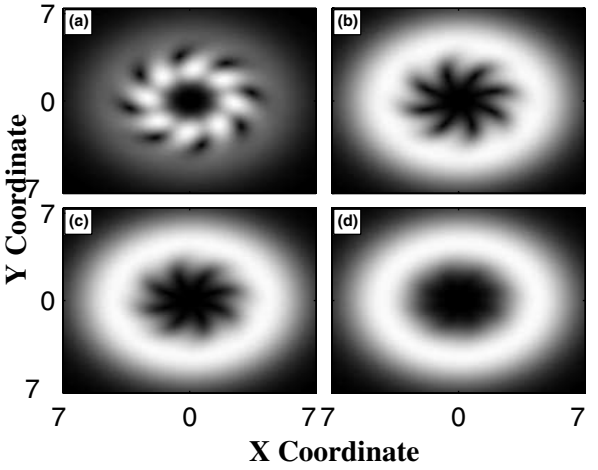


Figure 3. Analogous to figure 2 but for different $A_{0,2}$ values (conditions: input topological charges of the pump and seed beams, $[m_{\mathrm{FF}}, m_{\mathrm{SH}}] = [2, -4]$; $A_{\mathrm{FF}} = 0.1$; $w_{\mathrm{FF}} = 2$, $w_{\mathrm{SH}} = 3$) : (*a*) $A_{0,2} = 0.001$; (*b*) $A_{0,2} = 0.02$; (*c*) $A_{0,2} = 0.04$; (*d*) $A_{0,2} = 0.1$.

long. The crystal was heated in an oven and oriented for phase-matched type I non-critical SHG. The pump FF and seed SH input signals were prepared by splitting 1.1 ps (full width at half-maximum (FWHM)) pulses from a mode-locked neodymium-glass laser at the FF wavelength 1055 nm over two different beam-shaping lines. In one of the arms, a potassium dihydrogen phosphate (KDP) crystal was used to double the frequency of the incoming pulse. A series of dielectric mirrors with high reflectivity for the SH wavelength and an infrared absorbing filter were used after the KDP crystal to eliminate the remaining infrared radiation. A delay line was placed in the same optical path to optimize

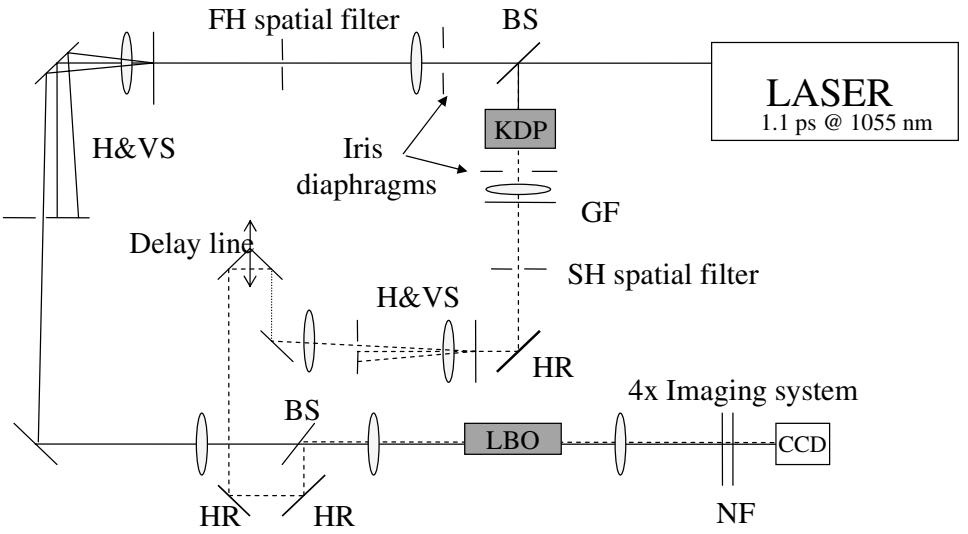


Figure 4. Experimental set-up: BS, beam splitter; H&VS, hologram and vortex selector; GF, green filter; NF, neutral filter; HR, high-reflectivity mirror.

the temporal overlap between the pulses. Multiple-charge optical vortices were nested in both the FF beam and the SH beam by high-diffraction efficiency computer-generated holograms; a pinhole was needed to select the desired diffraction order. Both beam-shaping lines included also a spatial filter to minimize noise and beam ellipticity and a lens telescope to obtain vortex beams with the desired beam waist. The two beams were joined together by means of a dichroic mirror and focused on the input face of the LBO crystal.

The peak power of the pump beam was controlled to ensure that SHG generation occurred well inside the low-depletion regime. We checked this point by comparing the input and output FF beams and verifying that the output signal was related to the input by pure diffraction. Finally, a charge-coupled device (CCD) imaging system placed right after the LBO crystal allowed the output light intensity distribution at the SH frequency band to be monitored.

Figure 5 shows illustrative examples of the output light intensity obtained at the SH frequency, for different combinations of the input values of $m_{\mathrm{FF}}$ and $m_{\mathrm{SH}}$. Numerical investigation predicts that the dark regions of the images are occupied by optical vortices. The experimental observation that the patterns were stable through propagation in air is a signature of this singular nature of the dark zones. Because the measurements were carried out under conditions of low depletion of the pump beam, the total SH output beam is approximately given by the superposition of the seed and the generated signal, and the output SH beam exhibits an $n$-fold azimuthal symmetry, with $n = |2m_{\mathrm{FF}} - m_{\mathrm{SH}}|$.

Figure 5 (*a*) corresponds to a setting with $n = 2$ obtained with input signals carrying vortices with topological charges $\mathrm{m_{FF}} = 0$ and $\mathrm{m_{SH}} = -2$. As visible in the image, two single-charge vortices located off-axis generate dark spots on the light intensity, producing a light intensity with a peanut shape. With the theoretical predictions reviewed in the previous section and series of numerical simulations [14, 15], one readily understands the phenomena taking place inside the crystal which finally leads to the observed output beam. The two off-axis vortices carry a

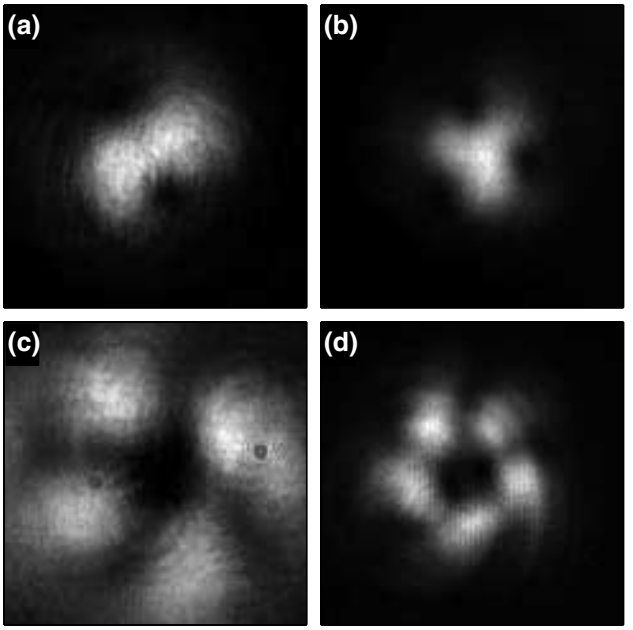


Figure 5. A sample of different geometries which can be obtained by mixing pump and seed beams with various combinations of topological charges: (*a*) $m_{FF} = 0$, $m_{SH} = -2$; (*b*) $m_{FF} = 0$, $m_{SH} = -3$; (*c*) $m_{FF} = +1$, $m_{SH} = -2$; (*d*) $m_{FF} = +1$, $m_{SH} = -3$. The overall power of FF and SH fields was always kept in the range of kilowatts in order to avoid FF depletion. The input diameters of the FF and SH ranged form 50 to 100 μm, depending on the topological charge nested in it. Zones displayed in white are the more intense.

negative topological charge and are produced by the splitting of the input vortex with charge $m_{SH} = -2$. The splitting is induced by the interference between the seed and generated SH beams. Similar input light conditions, but with $m_{FF} = 0$ and $m_{SH} = -3$, produce the $n = 3$ light pattern shown in figure 5 (*b*). In both cases, detailed theoretical investigations of the process predict the existence of additional sets of vortices located far from the beam waist where the light intensity is negligible. The images shown in figures 5 (*c*) and 5 (*d*) correspond to patterns of light with $n = 4$ and $n = 5$ respectively obtained under conditions which were engineered so that the output SH beam features an on-axis vortex, in addition to different sets of off-axis vortices. The image shown in figure 5 (*c*) was generated by an on-axis vortex of charge +2 surrounded by four vortices with charge −1 located symmetrically at about the beam waist. Note the dark lines that partition the beam in four pieces. They were generated by the four single-charge vortices generated when they move outwards off the beam axis. A similar vortex inventory is responsible for the $n = 5$ image shown in figure 5 (*d*). Additional examples of possible patterns are shown in figures 6 and 7.

Figure 8 shows representative experimentally observed examples of the reconfigurable beam shaping. Figures 8 (*a*) and (*b*) are to be compared with figure 5 (*a*), and figures 8 (*c*) and (*d*) are to be compared with figure 5 (*b*). The images demonstrate that, by changing the intensity of either the seed beam or the pump beam, the transverse location of the vortices existing in the beam at the position of

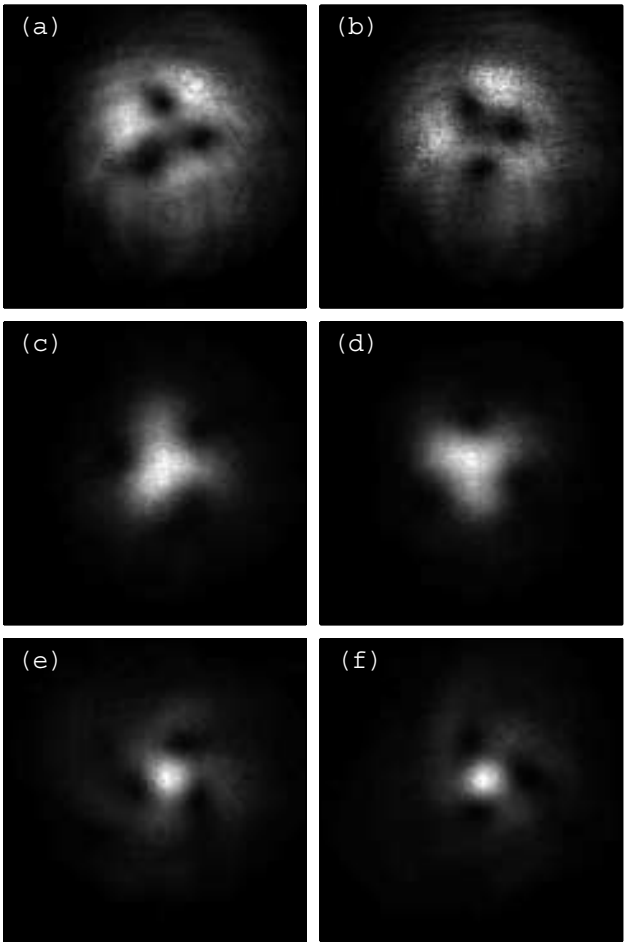


Figure 6. Different possibilities of beam shaping for a given geometry. Each row presents two different shots for the same initial conditions. Input topological charges are $m_{FF} = 0$ and $m_{SH} = -3$. Beam powers and widths are of the same order as in figure 5, but the relative amplitudes of the beams changes from row to row.

the CCD image acquiring system can be varied. Hence, the output light pattern can be reconfigured dynamically.

As expected from the very nature of the seeded SHG mechanism explored here, the azimuthal symmetry of the acquired light patterns was observed to be sensitive to the alignment between the pump and the seed beams. We conclude from our series of experiments that controlling the alignment of the input beams within some milliradians and the temporal and spatial overlap within a small fraction of the input pulse width and waist is required to obtain the output light pattern predicted under ideal conditions. Otherwise, important distortions of the shapes of the output the beams were observed to occur. Similarly, the transverse orientation of the output light pattern was observed to vary from shot to shot. A typical example is obtained by comparing right- and left-hand columns in figure 6. We attribute the observed azimuthal jitter to air turbulence, which modified in an unpredictable way the optical path along the arms of the pump and seed beams,

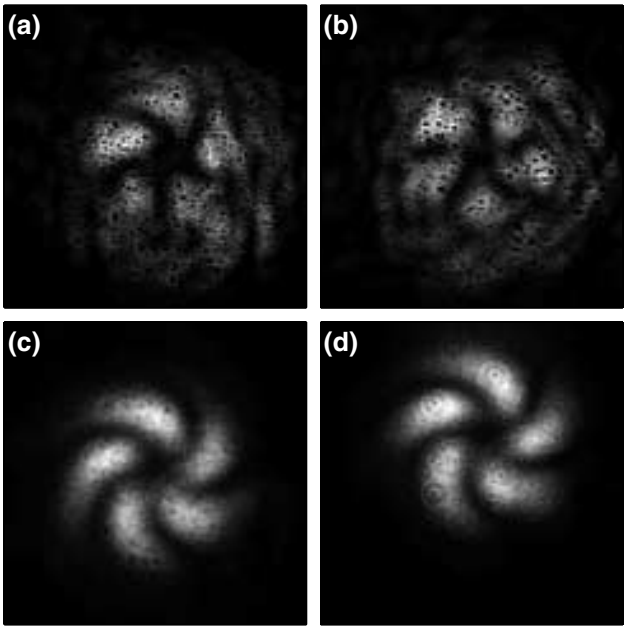


Figure 7. Beam shaping under conditions of small FF depletion. Input topological charges are $m_{\mathrm{FF}} = +1$ and $m_{\mathrm{SH}} = -3$. The left- and right-hand rows represent the SH and FF output beams respectively. Beam powers and widths are of the same order as in figure 5, although in this case FF depletion was observed. The relative amplitudes of the beams change from row to row.

and thus their relative phases. However, we anticipate that such jitter can be reduced drastically by shortening the length of each arm (in our setting, the arms were about 2 m long) and protecting the beam paths from air currents with a suitable sealing. Advanced solutions may use optical fibres to carry the light signals along each arm. Finally, we note that the output light pattern was observed to be robust against reasonable variations of the input light power. In our scheme the laser peak power varied by some 20% from shot to shot, and yet the shape of the pattern of output light intensity was observed to be stable.

## 4. Concluding remarks

In conclusion, we have discussed the simultaneous frequency doubling and dynamic shaping of beams into a variety of dynamically varying light patterns in seeded parametric wave-mixing schemes with focused input beams containing optical vortices. The experimental observations reported here were performed under conditions of SHG in LBO, but we note that the scheme can be potentially extended to all parametric processes and suitable materials with high quadratic nonlinearities.

Interesting possibilities for research include the implementation of the scheme with continuous-wave pump lasers, and in periodically poled materials with high quadratic nonlinearities, such as lithium niobate or potassium tytanil phosphate, where one can also benefit from quasiphase-matching engineering. It should be remarked that the technique can also be realized by the superposition of the

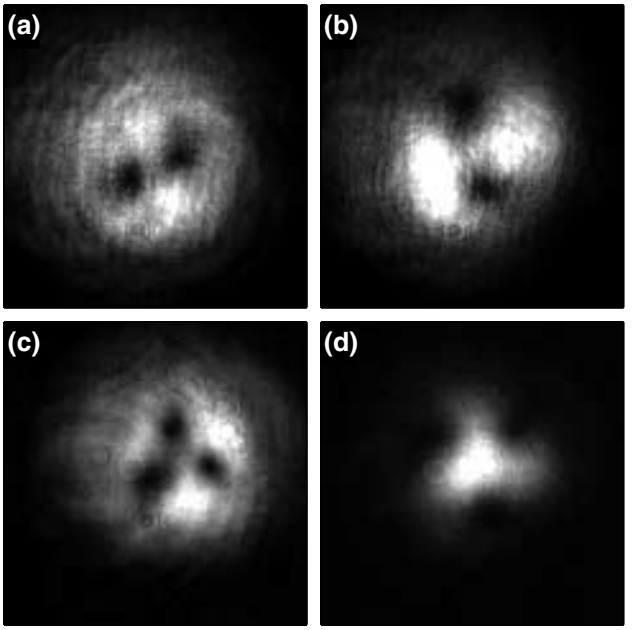


Figure 8. Effect of the input relative power between FF and SH fields where in all cases, $m_{FF} = 0$: (*a*) $d_{FF} = 50\,\mu m$ FWHM, $P_{FF} = 12\,kW$, $m_{SH} = -2$, $d_{SH} = 83\,\mu m$ FWHM and $P_{SH} = 1\,kW$; (*b*) $d_{FF} = 50\,\mu m$ FWHM, $P_{FF} = 12\,kW$, $m_{SH} = -2$, $d_{SH} = 83\,\mu m$ FWHM and $P_{SH} = 0.4\,kW$; (*c*) $d_{FF} = 60\,\mu m$ FWHM, $m_{SH} = -3$, $d_{SH} = 150\,\mu m$ FWHM, $P_{SH} = 1.3\,kW$ and $P_{FF} = 1.1\,kW$; (*d*) $d_{FF} = 60\,\mu m$ FWHM, $m_{SH} = -3$, $d_{SH} = 150\,\mu m$ FWHM, $P_{SH} = 1.3\,kW$ and $P_{FF} = 4.9$ kW.

generated and corresponding seed SH beams at the end of the crystal instead of at the input, even though in practice the seeded scheme appears to be more robust.

Applications might include the generation of dynamic patterns of frequency-converted coherent optical-tweezers patterns aimed at applications in nanotechnologies, including the assembly, fabrication and manipulation of micromachines, colloidal particles and complex photonic structures in settings which can benefit from wavelength-optimized pump light. For example, the fabrication of three-dimensional photonic structures along the lines put forward recently by Dholakia and co-workers [13] using light patterns generated by suitable combinations of Laguerre–Gaussian modes, but with wavelength-converted light signals, is a fascinating possibility for investigation.

## Acknowledgments

This work was supported by the Generalitat de Catalunya and by the Spanish Government through contract TIC2000-1010. We are grateful to Dr Kishan Dholakia (University of St Andrews, UK) for his interest in this work.

## References

[1] Ashkin, A., 1999, *Optics Photonics News*, **10,** 41.
[2] Padgett, M. J., and Allen, L., 2000, *Contemp. Phys.*, **41,** 275.

[3] Maruo, S., Nakamura, O., and Kawata, S., 1997, *Optics Lett.*, **22,** 132.
[4] Witzgall, G., Vrijen, R., Yablonovitch, E., Doan, V., and Schwartz, B. J., 1998, *Optics Lett.*, **23,** 1745.
[5] Cumpston, B. H., Ananthavel, S. P., Barlow, S., Dyer, D. L., Ehrlich, J. E., and Erskine, L. L., 1999, *Nature*, **398,** 51.
[6] Galajda, P., and Ormos, P., 2001, *Appl. Phys. Lett.*, **78,** 249.
[7] Galajda, P., and Ormos, P., 2002, *Appl. Phys. Lett.*, **80,** 4653.
[8] Rubinstein-Dunlop, H., and Friese, M. E. J., 2002, *Optics Photonics News*, **13,** 22.
[9] Zemanek, P., Jonas, A., Sramek, L., and Liska, M., 1999, *Optics Lett.*, **24,** 1448.
[10] Mogensen, P. C., and Gluckstad, J., 2000, *Optics Commun.*, **175,** 75.
[11] Paterson, L., MacDonald, M. P., Arlt, J., Sibbett, W., Bryant, P. E., and Dholakia, K., 2001, *Science*, **292,** 912.
[12] Eriksen, R. L., Mogensen, P. C., and Gluckstad, J., 2002, *Optics Lett.*, **27,** 267.
[13] MacDonald, M. P., Paterson, L., Volke-Sepulveda, K., Arlt, J., Sibbett, W., and Dholakia, K., 2002, *Science*, **296,** 1101.
[14] Molina-Terriza, G., and Torner, L., 2000, *J. opt. Soc. America* B, **17,** 1197.
[15] Molina-Terriza, G., and Torner, L., 2001, *Optics Lett.*, **26,** 154.
[16] Molina-Terriza, G., Minardi, S., Bramati, A., Di Trapani, P., and Torner, L., 2001, *Optics Express*, **9,** 110.
[17] Abramochkin, E., and Volostnikov, V., 196, 1996, *Optics Commun.*, **125,** 302.
[18] Abramochkin, E., Losevsky, N., and Volostnikov, V., 1997, *Optics Commun.*, **141,** 59.
[19] Gur, I., and Mendlovic, D., 1998, *Optics Commun.*, **145,** 237.
[20] Churin, E. G., 1999, *Optics Lett.*, **24,** 620.
[21] Freund, I., 1999, *Optics Commun.*, **159,** 99.
[22] Freund, I., 2000, *Optics Commun.*, **181,** 19.
[23] Allen, L., Padgett, M. J., and Babiker, B., 1999, *Prog. Optics*, **39,** 291.
[24] Kivshar, Yu. S., and Ostrovskaya, E. A., 2001, *Optics Photonics News*, **12,** 24.
[25] Soskin, M. S., and Vasnetsov, M. V., 2001, *Prog. Optics*, **42,** 219.
[26] Bazhenov, V. Yu. Vasnetsov, M. V., and Soskin, M. S., 1990, *JETP Lett.*, **52,** 429.
[27] Heckenberg, N. R., McDuff, R., Smith, C. P., and White, A. G., 1992, *Optics Lett.*, **17,** 221.
[28] Basistiy, I. V., Bazhenov, V. Yu., Soskin, M. S., and Vasnetsov, M. V., 1993, *Optics Commun.*, **103,** 422.
[29] Dholakia, K., Simpson, N. B., Padgett, M. J., and Allen, L., 1996, *Phys. Rev.* A, **54,** 3742.
[30] Petrov, D. V., Molina-Terriza, G., and Torner, L., 1999, *Optics Commun.*, **162,** 357.